System Size, Energy and Centrality Dependence of Pseudorapidity Distributions of Charged Particles in Relativistic Heavy Ion Collisions

B.Alver[4], B.B.Back[1], M.D.Baker[2], M.Ballintijn[4], D.S.Barton[2], R.R.Betts[6], R.Bindel[7], W.Busza[4], Z.Chai[2], V.Chetluru[6], E.García[6], T.Gburek[3], K.Gulbrandsen[4], J.Hamblen[8], I.Harnarine[6], C.Henderson[4], D.J.Hofman[6], R.S.Hollis[6], R.Hołyński[3], B.Holzman[2], A.Iordanova[6], J.L.Kane[4], P.Kulinich[4], C.M.Kuo[5], W.Li[4], W.T.Lin[5], C.Loizides[4], S.Manly[8], A.C.Mignerey[7], R.Nouicer[2], A.Olszewski[3], R.Pak[2], C.Reed[4], E.Richardson[7], C.Roland[4], G.Roland[4], J.Sagerer[6], I.Sedykh[2], C.E.Smith[6], M.A.Stankiewicz[2], P.Steinberg[2], G.S.F.Stephans[4], A.Sukhanov[2], A.Szostak[2], M.B.Tonjes[7], A.Trzupek[3], G.J.van Nieuwenhuizen[4], S.S.Vaurynovich[4], R.Verdier[4], G.I.Veres[4], P.Walters[8], E.Wenger[4], D.Willhelm[7], F.L.H.Wolfs[8], B.Wosiek[3], K.Woźniak[3], S.Wyngaardt[2], B.Wysłouch[4]

[1] Argonne National Laboratory, Argonne, IL 60439-4843, USA
[2] Brookhaven National Laboratory, Upton, NY 11973-5000, USA
[3] Institute of Nuclear Physics PAN, Kraków, Poland
[4] Massachusetts Institute of Technology, Cambridge, MA 02139-4307, USA
[5] National Central University, Chung-Li, Taiwan
[6] University of Illinois at Chicago, Chicago, IL 60607-7059, USA
[7] University of Maryland, College Park, MD 20742, USA
[8] University of Rochester, Rochester, NY 14627, USA

(Dated: October 3, 2007)

We present the first measurements of the pseudorapidity distribution of primary charged particles in Cu+Cu collisions as a function of collision centrality and energy, $\sqrt{s_{NN}} = 22.4$, 62.4 and 200 GeV, over a wide range of pseudorapidity, using the PHOBOS detector. Making a global comparison of Cu + Cu and Au + Au results, we find that the total number of produced charged particles and the rough shape (height and width) of the pseudorapidity distributions are determined by the number of nucleon participants. More detailed studies reveal that a more precise matching of the shape of the Cu + Cu and Au + Au pseudorapidity distributions over the full range of pseudorapidity occurs for the same $N_{part}/2A$ value rather than the same N_{part} value. In other words, it is the collision geometry rather than just the number of nucleon participants that drives the detailed shape of the pseudorapidity distribution and its centrality dependence at RHIC energies.

PACS numbers: 25.75.-q, 25.75.Dw

The advent of Cu + Cu collisions from the Relativistic Heavy Ion Collider (RHIC) at energies similar to those of the earlier Au + Au collisions presents a new opportunity to measure the system size dependence of important observables using different collision geometries. The Cu + Cu results are expected to provide critical tests of the parametric dependence of the pseudorapidity density of charged particles, $dN_{ch}/d\eta$, observed previously in Au + Au collisions [1–3]. They significantly extend the range of measurements with respect to the number of participant nucleons, N_{part}, compared to Au + Au and also allow for a direct comparison at the same N_{part}.

The observed $dN_{ch}/d\eta$ is a conceptually well-defined quantity that reflects most effects that contribute to particle production in heavy-ion collisions. It is sensitive to the initial conditions of the system, i.e. parton shadowing, and also to the effects of rescattering and hadronic final-state interactions. In short, the full distribution of $dN_{ch}/d\eta$ represents a time-integral of particle production throughout the entire heavy-ion collision.

In this letter, we present the first measurements of the $dN_{ch}/d\eta$ of primary charged particles over a broad range, $|\eta| < 5.4$, for Cu + Cu collisions at a variety of collision centralities. These measurements were made in the same detector for $\sqrt{s_{NN}}$= 22.4, 62.4 and 200 GeV allowing for a reliable systematic study of particle production as a function of energy. The Cu + Cu results are compared to results from Au + Au [2, 3] and d+Au collisions [4, 5] at similar energies obtained with the same detector. This led us to perform a comprehensive examination of particle production in Cu + Cu and Au + Au collisions for the same number of nucleon participant pairs and for the same fraction of total cross section in both systems, and to study the interplay between energy and system size.

The data were obtained with the multiplicity array of the PHOBOS detector [6] during the RHIC 2005 run. This array is identical to that used in our study of Au + Au and d+Au collisions [2–5]. Monte Carlo simulations of the detector performance were based on the HIJING event generator [7] and GEANT [8] simulations, folding in the signal response for scintillator counters (Paddles, covering $3.0 < |\eta| < 4.5$), and silicon sensors.

The Au + Au data at $\sqrt{s_{NN}}$= 19.6, 62.4 and 200 GeV used in this paper for comparison with Cu + Cu results were taken with the PHOBOS detector [2, 3]. In the

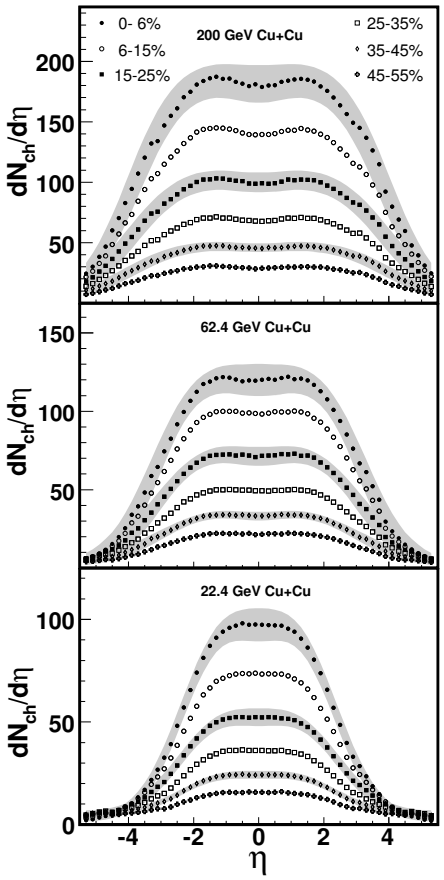

FIG. 1: $dN_{ch}/d\eta$ distributions of primary charged particles from Cu + Cu collisions at $\sqrt{s_{NN}}$ = 22.4, 62.4, and 200 GeV for the specified centrality bins. The typical systematic errors (90% C.L.) are shown as bands for selected centrality bins.

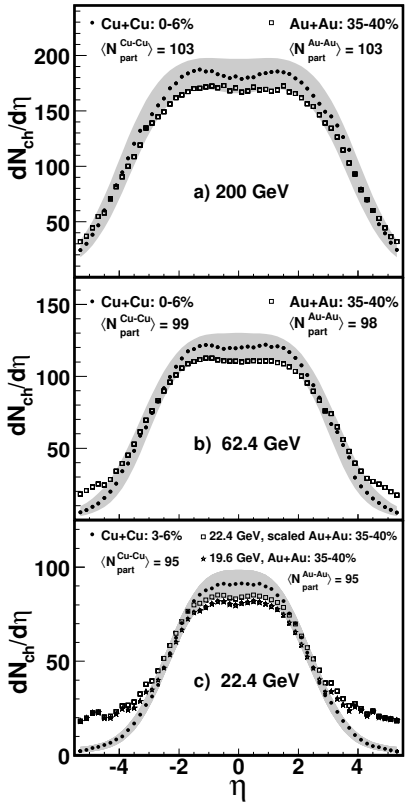

FIG. 2: $dN_{ch}/d\eta$ distributions in Cu+Cu and Au+Au [2, 3] collisions selected to yield similar $\langle N_{part}\rangle$, a) at 200 GeV, b) at 62.4 GeV and c) at 22.4 GeV. The grey band indicates the systematic uncertainty (90% C.L.) for Cu+Cu. Errors for Au + Au are not shown for clarity.

present work, the Au + Au data at 19.6 GeV have been reanalyzed using an improved treatment of dead detector channels, resulting in slightly smaller multiplicity than given in previous publications. However, the $dN_{ch}/d\eta$ distributions shown in the present work and those published in Refs. [2, 3] agree within the systematic errors. The 19.6 Au + Au data and the new Cu + Cu data were analyzed in the same way as the previously published data of Au + Au at 200 and 62.4 GeV [2, 3], using two analysis methods [9], "hit-counting" and "analog". In the present work, the analog results were corrected for the over-counting of multiply-charged fragments such as He emitted in the forward regions. The correction, which was largest for the lowest energies and most peripheral collisions, changed the total number of charged particles by less than 6%, and has been taken into account in the systematic error assignments.

The centrality determination procedure applied for Cu + Cu collisions is the same as for Au + Au collisions at similar energies [2, 3]. For the 200 and 62.4 GeV data sets, the centrality was estimated from the data using the truncated mean of the Paddles signals. Using several methods, based on the HIJING [7] and AMPT [10] models, we have estimated our minimum-bias trigger efficiency for events with a vertex near the nominal interaction point to be $84 \pm 5\%$ and $75 \pm 5\%$ in Cu + Cu collisions at 200 and 62.4 GeV, respectively. At the lowest energies, 22.4 GeV (Cu + Cu) and 19.6 GeV (Au + Au), the much lower beam rapidity ($y_{beam} \sim 3$) precludes the use of the Paddles for centrality determination. Instead, we construct a different quantity, "EOCT", the path-length-corrected sum of the energy deposited in the Octagon (silicon) detector ($|\eta| \leq 3.2$). This procedure has been discussed in detail in Ref. [2]. We use a Glauber model calculation implemented in HIJING simulations to estimate $\langle N_{part}\rangle$ for each centrality bin. The $\langle N_{part}\rangle$ values for various centrality bins for Cu + Cu collisions are given in Table I.

Figure 1 shows the primary charged particle $dN_{ch}/d\eta$ distributions measured in Cu + Cu collisions at $\sqrt{s_{NN}}$= 22.4, 62.4, and 200 GeV for different centrality bins. The statistical errors are negligible. Both the height and width of the $dN_{ch}/d\eta$ distributions increase as a function of energy as has been seen for Au + Au collisions [2].

The comparison of $dN_{ch}/d\eta$ distributions for Cu + Cu

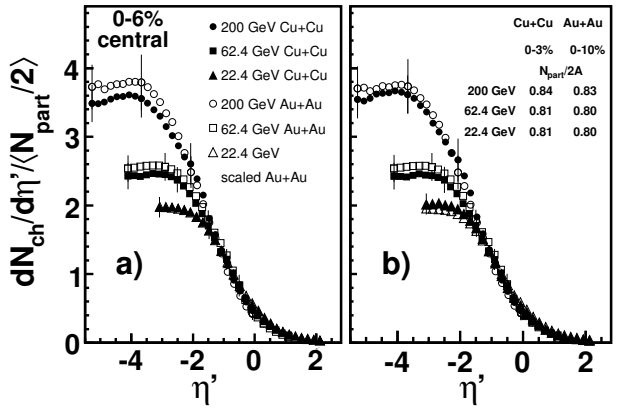

FIG. 3: Cu + Cu and Au + Au [3] data at RHIC energies, plotted as $dN_{ch}/d\eta'/\langle N_{part}/2\rangle$, where $\eta' \equiv \eta - y_{beam}$, for a) 0–6% most central events and b) events with similar value of $N_{part}/2A$. For the 0-6% central collisions of Cu + Cu (Au + Au) at 200, 62.4 and 22.4 (19.6) GeV, the values of $N_{part}/2A$ are 0.82 (0.87),0.78 (0.85) and 0.78 (0.86), respectively. Systematic errors (90% C.L.) are shown for typical points.

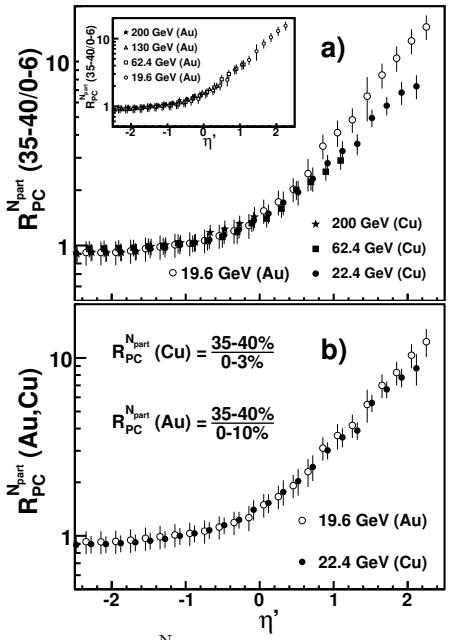

FIG. 4: The ratio, $R_{PC}^{N_{part}}(\eta')$, of $dN_{ch}/d\eta'/\langle N_{part}/2\rangle$ for Cu + Cu and Au + Au collisions at RHIC energies, a) comparing the 35–40% bin to the 0-6% most central bin and b) $R_{PC}^{N_{part}}(\eta')$ for Cu + Cu and Au + Au for centrality bins selected such that $N_{part}/2A$ is similar for the two systems. The inset figure (a) represents the $R_{PC}^{N_{part}}(\eta')$ only for Au + Au data for four different energies [3]. The errors represent a 90% C.L. systematic error on the ratio. Note : the scaled Au + Au at 22.4 GeV has not been added in the figure because the ratio, $R_{PC}^{N_{part}}(\eta')$, for a given system is independent of energy. The values of $N_{part}/2A$ are given in Fig. 3 and the value of $N_{part}/2A$ for Cu + Cu and Au + Au for 35-40% collisions centrality at 22.4 (19.6) GeV are both equal to 0.24.

and Au + Au collisions at the same energy, for centrality bins chosen so that the average number of participants in both systems is similar, is presented in Fig. 2. No scaling factors are applied. At 200 GeV, Fig. 2a, the $dN_{ch}/d\eta$ distributions in both systems at similar $\langle N_{part}\rangle$ agree within systematic errors, both in height and width. At 62.4 and 22.4 GeV, Fig. 2b and c, we observe that the distributions agree within systematic errors at midrapidity but not in the fragmentation regions (i.e. high $|\eta|$). The $dN_{ch}/d\eta$ distributions of Au + Au collisions at 19.6 and 62.4 GeV have been interpolated linearly in $\ln(\sqrt{s_{NN}})$ to obtain the scaled Au + Au data at 22.4 GeV. The fragmentation region dependence on the size of the colliding nuclei is exhibited through increased charged particle production in Au + Au as compared to Cu + Cu collisions which may be attributed to the two excited nuclear remnants being bigger in Au + Au than in Cu + Cu collisions. This effect is most visible at the lowest energies where the broad η coverage gives access to $|\eta| > y_{beam}$.

The interplay between the system size and the collision energy is shown in Fig. 3. It shows the scaled pseudorapidity particle densities, $dN_{ch}/d\eta'/\langle N_{part}/2\rangle$ (where $\eta' \equiv \eta - y_{beam}$ corresponds effectively to the rest frame of one of the colliding nuclei [1, 2]) for Cu + Cu and Au + Au collisions for centrality bins with a) the same fraction of total cross section 0-6% and b) similar value of $N_{part}/2A$, where A is the mass number of the colliding nuclei. It should be noted that systems with matching $N_{part}/2A$ values will also have matching N_{spec}/N_{part} values, where N_{spec} = 2A - N_{part} is the number of non-participating nucleons (spectators). The results shown in Fig. 3 suggest that in symmetric nucleus-nucleus collisions the particle density per nucleon participant pair at the midrapidity region does not depend on the size of the two colliding nuclei but only on the collision energy and geometry. In the fragmentation region, the phenomenon of extended longitudinal scaling observed in Au + Au [1, 2] and d + Au [5] collisions is also present in the Cu + Cu data. The Cu + Cu and Au + Au collisions exhibit the same extended longitudinal scaling in central collisions. This suggests that the extended longitudinal scaling holds independent of the collision energy and system size. The comparison presented in Fig. 3 reveals an interesting feature: for centrality bins corresponding to the same fraction of total cross section in Cu + Cu and Au + Au collisions and at similar energy, the $dN_{ch}/d\eta/\langle N_{part}/2\rangle$ distributions in both systems agree within errors over the full range of η. Slightly better agreement of $dN_{ch}/d\eta/\langle N_{part}/2\rangle$ distributions is obtained for centrality bins selected to yield similar value of $N_{part}/2A$ in both systems as presented in Fig. 3b.

To study the centrality dependence of extended longitudinal scaling in Cu + Cu and Au + Au collisions, we examine the ratios of $dN_{ch}/d\eta'/\langle N_{part}/2\rangle$ for central and

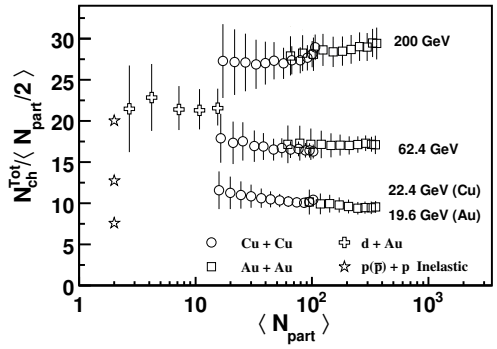

FIG. 5: The integrated total of primary charged particle production obtained by extrapolating the data at each energy into the unmeasured region is shown as a function of centrality in Cu + Cu collisions. The Au + Au, d+Au and inelastic $p(\bar{p})$ + p data are taken from Refs. [3, 5]. The uncertainty on N_{ch}^{Tot} and N_{part} has been included in the error bars.

semi-central, denoted $R_{PC}^{N_{part}}$, at different energies as a function of η'. The inset of Fig. 4a shows the previously published results for Au + Au collisions [3], indicating that the change in shape as a function of centrality is independent of beam energy. The ratios $R_{PC}^{N_{part}}$ for Cu + Cu at three energies exhibit the same feature (solid points) in Fig. 4a. By comparing to Au + Au results (open points) this ratio is found to be similar in the midrapidity region $-2.5 \leq \eta' \leq 0.5$ but in the region $\eta' > 0.5$ the ratio for Au + Au is higher. To study this difference, we plot in Fig. 4b the $R_{PC}^{N_{part}}$ ratio for Cu + Cu and Au + Au for centrality bins selected to represent similar initial geometry even more precisely, i.e. similar value of $N_{part}/2A$ for the two systems. Using this comparison criterion we observe good agreement between the two systems over the full range of pseudorapidity.

The values of total charged particle multiplicity, N_{ch}^{Tot}, estimated by extrapolation to the unmeasured region of pseudorapidity, are presented for Cu + Cu collisions at $\sqrt{s_{NN}}$ = 22.4, 62.4 and 200 GeV in Fig. 5 and given in Table I. The method used to determine N_{ch}^{Tot} is detailed in Ref. [12] for Au + Au collisions. At all energies, N_{ch}^{Tot} is obtained by averaging the results of two techniques. One involved fitting a Wood-Saxon functional form to the data for $|\eta| \leq 8$ at the two higher energies and $|\eta| \leq y_{beam}$ at the lowest energy where y_{beam}^{CuCu}(22.4 GeV) = 3.2 and y_{beam}^{AuAu}(19.6 GeV) = 3.0. The other involved simply integrating the lowest energy data and using the extended longitudinal scaling result to extrapolate the higher energy data into the unmeasured regions. The Cu + Cu and Au + Au results are compared at the same energies, 62.4 and 200 GeV, as well as at nearly the same energy 22.4 (CuCu) and 19.6 GeV (Au + Au) in Fig. 5. We observe that N_{ch}^{Tot} scales approximately linearly with $\langle N_{part} \rangle$ in both Cu + Cu and Au + Au collisions, and has similar values for the same $\langle N_{part} \rangle$. The comparison indicates that the transition between inelastic $p(\bar{p})$ + p and Cu + Cu collisions is not controlled simply by the number of participants, as even the very central d + Au multiplicity per participant pair shows little sign of continuity to the Cu + Cu results.

In summary, the measured pseudorapidity distributions of charged particles and the estimated total charged particle multiplicity in Cu + Cu collisions are presented as a function of collision centrality and energy, $\sqrt{s_{NN}}$= 22.4, 62.4 and 200 GeV. The results show that N_{part} is the scaling variable unifying the centrality dependence for Cu + Cu and Au + Au in the midrapidity region and for N_{ch}^{Tot}. However, the best agreement of the pseudorapidity distributions per nucleon participants over the full range of η between Cu + Cu and Au + Au in the central collisions at the same energy is obtained for centrality bins selected to yield similar value of $N_{part}/2A$ in both systems. The Cu + Cu and Au + Au results at similar energy show that the particle density per nucleon participant pair in the midrapidity region is similar in both systems. The phenomenon of extended longitudinal scaling in Cu + Cu and Au + Au collisions holds independent of colliding energy and system size. A dependence on the size of the colliding nuclei is observed in the pseudorapidity distributions in the fragmentation region at low energies, 22.4 (Au + Au 19.6) and 62.4 GeV, when the collision centrality of the two systems is selected for similar N_{part}. This may be attributed to the two excited nuclear remnants being bigger in Au + Au than in Cu + Cu collisions. The essential role of collision geometry when comparing pseudorapidity distributions of charged particles between nuclear species is clearly demonstrated.

This work was partially supported by U.S. DOE grants DE-AC02-98CH10886, DE-FG02-93ER40802, DE-FG02-94ER40818, DE-FG02-94ER40865, DE-FG02-99ER41099, and DE-AC02-06CH11357, by U.S. NSF grants 9603486, 0245011, 1-P03B-062-27(2004-2007), by NSC of Taiwan Contract NSC 89-2112-M-008-024, and by Hungarian OTKA grant (F049823).

[1] I. G. Bearden *et al.*, Phys. Rev. Lett. **88**,202301 (2002).
[2] B. B. Back *et al.*, Phys. Rev. Lett. **91**, 052303 (2003).
[3] B. B. Back *et al.*, Phys. Rev. C **74**, 021901 (2006).
[4] B. B. Back *et al.*, Phys. Rev. Lett. **93**, 082301 (2004).
[5] B. B. Back *et al.*, Phys. Rev. C **72**, 031901(R) (2005).
[6] B. B. Back *et al.*, Nucl. Instr. Meth. A **499**, 603 (2003).
[7] M. Gyulassy *et al.*, Phys. Rev. D **44**, 3501 (1991).
[8] GEANT 3.211, CERN Program Library.
[9] B. B. Back *et al.*, Phys. Rev. Lett. **87**, 102303 (2001).
[10] Zi-wei Lin *et al.*, Nucl. Phys. A **698**, 375 (2002).
[11] B. B. Back *et al.*, Nucl. Phys A **757**, 28 (2005).
[12] B. B. Back *et al.*, Phys. Rev. C **74**, 021902(R) (2006).

TABLE I: The estimated number of nucleon participants, $\langle N_{part} \rangle$, and the total charged particle multiplicity, N_{ch}^{Tot}, extrapolated to the unmeasured region for Cu+Cu collisions in different centrality bins are presented. All errors are systematic (90% C.L.).

Centrality	200 GeV		62.4 GeV		22.4 GeV	
Bin (%)	$\langle N_{part} \rangle$	N_{ch}^{Tot}	$\langle N_{part} \rangle$	N_{ch}^{Tot}	$\langle N_{part} \rangle$	N_{ch}^{Tot}
0–3	106 ± 3	1541 ± 70	102 ± 3	833 ± 36	103 ± 3	535 ± 23
3–6	100 ± 3	1407 ± 68	95 ± 3	781 ± 34	95 ± 3	482 ± 21
6–10	91 ± 3	1262 ± 59	88 ± 3	721 ± 32	86 ± 3	431 ± 19
10–15	79 ± 3	1084 ± 51	76 ± 3	635 ± 27	74 ± 3	375 ± 18
15–20	67 ± 3	917 ± 43	65 ± 3	541 ± 24	63 ± 3	320 ± 15
20–25	57 ± 3	771 ± 38	55 ± 3	460 ± 21	53 ± 3	273 ± 14
25–30	47 ± 3	645 ± 32	47 ± 3	386 ± 17	44 ± 3	230 ± 13
30–35	40 ± 3	538 ± 27	38 ± 3	323 ±15	37 ± 3	194 ± 12
35–40	33 ± 3	444 ± 23	32 ± 3	270 ± 13	30 ± 3	162 ± 12
40–45	27 ± 3	364 ± 19	25 ± 3	223 ± 11	25 ± 3	135 ± 11
45–50	22 ± 3	293 ± 15	21 ± 3	183 ± 9	20 ± 3	112 ± 11
50–55	17 ± 3	234 ± 13	16 ± 3	147 ± 8	16 ± 3	92 ± 11